

## COLOR GRADIENTS IN GALAXIES OUT TO $Z \sim 3$ : DEPENDENCE ON GALAXY PROPERTIES

NIRAJ WELIKALA<sup>1</sup>, JEAN-PAUL KNEIB<sup>2</sup>  
*Draft version April 16, 2019*

### ABSTRACT

Using HST/ACS observations, we measure the color gradients of 3248 galaxies in the GOODS-South field out to  $z \sim 3$  and  $i_{AB} < 25.5$  and characterize their dependence on galaxy properties (luminosity, apparent magnitude, galaxy size, redshift and morphological type). The color gradient is measured by the difference of  $v-i$  color outside ( $R_{50} \leq r < 2R_{50}$ ) and inside the half light radius. The gradient shows little evolution with redshift up to  $z \sim 1$  but increases from  $z \sim 1$  to  $z \sim 2$  before flattening out. It also increases with apparent magnitude, with a median value of 0.24 magnitudes at  $i_{AB} \sim 25.5$ . It has a strong color dependence, with the bluest galaxies (in terms of observed color) having cores that are bluer relative to their outskirts. We probe the redshift evolution by stacking galaxies and measuring the radial variation of  $v-i$  within them. At low redshifts ( $z < 0.5$ ), the centres of galaxies ( $r < R_{50}$ ) are slightly redder than their outskirts ( $1.5R_{50} \leq r < 2R_{50}$ ). Galaxies at  $z \sim 1$  and  $-22.0 < M_I \leq -21.0$  are bluer in their cores by 0.1 magnitudes, on average, compared to their outskirts. For  $z > 1$ , galaxies show increasingly bluer cores while the color of the outskirts does not change as rapidly. At  $z \sim 2.5$  and  $-22.0 < M_I \leq -21.0$ , we observe a difference, on average, of 0.4 magnitudes between the centre and the outskirts. The observed color gradients may indicate that strong star formation in galaxies at  $z \gtrsim 2$  is concentrated in their central regions. These color gradients and their dependence on observable properties could also have a significant impact on shear measurements in upcoming weak lensing cosmological surveys.

*Subject headings:* galaxies:evolution — galaxies:statistics — cosmology:systematics

### 1. INTRODUCTION

In order to provide useful constraints on dark energy, lensing surveys have to make very accurate determinations of galaxy shapes by correcting for the smearing effect of the Point Spread Function (PSF). The PSF determination is obtained generally from stars which have a bluer spectrum than faint distant galaxies. In addition, in galaxies, the spectrum can vary with the position in the galaxy image. Color gradients within galaxies can thus bias the shape measurements. Voigt et al. (2011) estimated this bias out to  $z \sim 1$  by modelling galaxies using two co-centered, co-elliptical Sersic profiles, each with a different spectrum. They showed that the shear bias from a single galaxy can be substantial depending on the properties of the galaxy and the width of the filter used. Using a small galaxy catalog from Simard et al. (2002) which was based on WFPC2 observations of the ‘Groth Strip’ (Groth et al. 1994, Rhodes, Refregier & Groth 2000) and which goes up to  $z \sim 1$  (median redshift of 0.65), they found a mean shear bias that is lower than the statistical errors for future cosmic shear surveys. However, the true mean shear bias may exceed the statistical errors depending on how accurately this catalog represents the observed distribution of galaxies in cosmic shear surveys. In this paper, we use a large galaxy sample (3248 objects down to  $i_{AB} = 25.5$  and  $z \sim 3$ ) in the GOODS-South field (Giavalisco et al. 2004) to characterize the color gradients in galaxies and their dependence on galaxy properties. The determination of these gradients for a large statistical sample will enable corrections to be made to this systematic in shear measurements.

The measurement of these gradients also has implications for the evolution of galaxies. By stacking galaxies in volume-limited subsamples, we also characterize the evolution of the radial color variation with redshift, from the local Universe out to  $z \sim 3$ . The relative difference in color between the interior of the galaxy and the outskirts, and its evolution with galaxy properties and in particular with redshift, indicates whether star formation in these galaxies occurs preferentially in the nucleus or the outskirts of the galaxies and if this location changes on average with redshift and other galaxy properties. Several studies of spatially resolved galaxy properties, including star formation, at  $z \sim 0.1$  have been performed by Welikala et al. (2008; 2009) and Park et al. (2007) in the Sloan Digital Sky Survey (SDSS; Abazajian et al. 2009). These studies have explored the relation between spatially resolved color (and hence stellar population) trends and the galaxy environment. Tortora et al. (2010; 2011) explored both color gradients and stellar M/L gradients in galaxies in SDSS and showed that M/L gradients are strongly correlated with color gradients. Suh et al. (2010) studied early-type galaxies drawn from the SDSS DR6 and found a strong correlation between the existence of steep colour gradients and ongoing residual star formation. They also showed that elliptical galaxies with bluer cores had global bluer colors than average. Lee et al. (2008) found that steeper colour gradients appear within star forming galaxies, in both late and early-types. Color gradients of low-redshift spiral galaxies appear to be dominated by the fact that, on average, their bulges are redder than their disks. However, this may be an oversimplification for many late-type galax-

<sup>1</sup> Insitut d’Astrophysique Spatiale, Bâtiment 121, Université Paris-Sud XI & CNRS, 91405 Orsay Cedex, France, niraj.welikala@ias.u-psud.fr  
<sup>2</sup> Laboratoire d’Astrophysique de Marseille, CNRS & Université Aix-Marseille, 38, rue Frédéric Joliot-Curie, 13388 Marseille Cedex 13, France, jean-paul.kneib@oamp.fr

ies (e.g., Bakos et al. 2008). Gonzalez-Perez et al. (2011) studied the relation between color gradients in galaxies at  $0.01 < z < 0.17$  in SDSS DR7 and their galactic properties. They found that, on average, galaxies in this redshift range have redder cores than their outskirts and found a steeper gradient in late-type galaxies than in early-types. They also demonstrated a connection between steep color gradients and a higher proportion of young stars within a galaxy, and found that nuclear activity is a marginal driver for creating steep color gradients in massive galaxies. However, the relation between color gradients and galaxy properties at higher redshifts have not been fully explored to date with large galaxy samples.

Some studies at higher redshifts have been performed using relatively small samples of galaxies. For example, Ferreras et al. (2005) studied the evolution of 249 field early-type galaxies in GOODS-South, with a median redshift of 0.71 and measured their color gradients. They found that red and blue early-type galaxies in their sample have distinct behavior with respect to their color gradients. In particular, they found that most blue early-type galaxies feature blue cores whereas most red early-types have passively evolving stellar populations with red cores, i.e., similar to local early-type galaxies. Furthermore, they found that, out to  $z \sim 1$ , color gradients and their scatter do not evolve with redshift and are compatible with the observations at  $z \sim 0$ , assuming a radial dependence of the metallicity within each galaxy. They also ruled out significant gradients in the stellar age out to  $z \sim 1$ . Brok et al. (2011) used deep, HST imaging to determine color profiles of early-type galaxies in the Coma cluster. They found negative color gradients for these galaxies and in addition, found that color profiles are typically linear as a function of  $\log(R)$ , sometimes with a nuclear region of distinct, often bluer color. They found that color gradients of dwarf galaxies form a continuous sequence with those of elliptical galaxies, becoming shallower toward fainter magnitudes. Using the colors as metallicity tracers, they suggested that dwarfs as well as giant early-type galaxies in the Coma cluster are less metal rich in their outer parts. They did not find evidence for the environment of galaxies impacting the gradients, although most of the galaxies in their sample were found in the central regions of the cluster. They also found that S0 galaxies in a subsample have less steep gradients than elliptical galaxies.

In this work, we are interested in the impact of color gradients out to higher redshifts ( $z \sim 3$ ) as would be observed by future deep and wide cosmological weak imaging lensing surveys such as the Dark Energy Survey (DES<sup>3</sup>; Wester et al. 2005), the Kilo-Degree Survey (KIDS<sup>4</sup>), the Hyper Suprime-Cam (HSC) Project<sup>5</sup>, the Large Synoptic Survey Telescope (LSST<sup>6</sup>; LSST Collaboration 2009), *Euclid*<sup>7</sup> (Laureijs et al. 2011) and the Wide-Field InfraRed Survey Telescope (*WFIRST*; Green et al. 2011). This relies on a large photometric galaxy sample out to high red-

shifts. The lensing shear measurements will be impacted by galaxies of varying types, luminosities, sizes and redshifts, and the aim of this paper is to explore for the first time these dependences that will affect the shape measurements of galaxies. In particular, lensing measurements and the impact of color gradients on these measurements have been studied in the context of the SNAP (SNAP Collaboration 2004) /JDEM project (Seiffert, private communication) and the *Euclid* project (e.g Voigt et al. 2011). For this reason, the *Euclid* Visible Channel (VIS) is also equipped with a narrow band filter that will enable the determination of the correction of the color gradient effect as a function of galaxy properties and redshift out to  $z \sim 3$ .

However, by exploring these trends, we also show trends in the color gradients that are directly related to star formation and possibly other astrophysical processes in galaxies. By stacking objects in volume-limited samples within our large sample, we also aim to investigate the evolution of the color gradient from the local Universe out to  $z \sim 3$ . This is likely to have an interpretation in terms of how star formation and feedback in galaxies evolve across cosmic time. We use the AB magnitude system throughout this paper.

## 2. THE PHOTOMETRIC SAMPLE

We use a magnitude-limited ( $i < 26$ ) sample of galaxies in the GOODS-South survey (Giavalisco et al. 2004) from version 2.0 of the publicly available ACS source catalog<sup>8</sup> as well as a photometric redshift galaxy catalog for CDFS (Cardamone et al. 2010). The ACS source catalog is produced using the SExtractor package (Bertin & Arnouts 1996). This also determine the position of the central pixel of each galaxy. We then produce a  $5'' \times 5''$  postage stamp cutout image of each galaxy from the reduced, calibrated, stacked and mosaiced ACS images<sup>9</sup> in the  $v606$  and  $i775$  passbands. We also apply a selection on galaxy size, as determined by tests described in Section 3.2. This leaves us with a photometric sample of 3248 galaxies with  $v$  and  $i$  band images.

In order to compare any systematic effect in the dependence of the color gradient on redshift due to the use of photometric redshifts as opposed to spectroscopic redshifts, we also select a subsample of the galaxies from our photometric catalog which fall in the GOODS-VIMOS spectroscopic campaign (Popesso et al. 2009; Balestra et al. 2010). This consists of two surveys which target galaxies in different redshift ranges. The VIMOS Low Resolution Blue (LR-Blue) is aimed at observing galaxies mainly at  $1.8 < z < 3.5$  while the Medium Resolution (MR) orange grism is aimed mostly at galaxies at  $z < 1$  and Lyman Break Galaxies (LBGs) at  $z > 3.5$ . These leave 531 galaxies with both spectroscopic and photometric redshifts for the comparison.

Figure 1 illustrates the selection of both samples in luminosity and redshift as well as in apparent magnitude

<sup>3</sup> <http://www.darkenergysurvey.org>

<sup>4</sup> <http://www.astro-wise.org/projects/KIDS/>

<sup>5</sup> <http://www.naoj.org/Projects/HSC/HSCProject.html>

<sup>6</sup> <http://www.lsst.org>

<sup>7</sup> <http://www.euclid-ec.org>

<sup>8</sup> [http://archive.stsci.edu/pub/hlsp/goods/catalog\\_r2](http://archive.stsci.edu/pub/hlsp/goods/catalog_r2)

<sup>9</sup> <http://archive.stsci.edu/pub/hlsp/goods/v2/>

and half light radius. The photometric sample is complete down to  $z \sim 2.5$  and  $M_I < -20.0$ , while the spectroscopic sample is complete down to  $z \sim 2$  and  $M_I < -21.0$ . The magnitude limit of the photometric sample is 25.5 while it is 24.5 for the spectroscopic sample.

Figure 2 illustrates the distribution of each of the galaxy properties being studied in the sample. In terms of photometric redshift, there are 638 galaxies at  $z < 0.5$ , 1195 galaxies at  $0.5 < z < 1.0$ , 768 galaxies at  $1.0 < z < 1.5$ , 320 galaxies at  $1.5 < z < 2.0$ . In particular, there are 277 galaxies in the redshift interval  $2.0 < z < 3.0$ , allowing a statistically significant evolution of the color gradient between  $z = 2$  and  $z = 3$ . The photometric redshift distributions of the early and late-type galaxy samples are also shown in Figure 2. The distribution of spectroscopic redshifts is also included. There are 109 objects in the spectroscopic sample in the redshift interval  $2 < z < 3$ , with a median redshift of 0.84.

1171 galaxies have  $i_{AB} > 24.0$ . 594 galaxies are in the absolute magnitude range  $-21.0 < M_I \leq -20.0$  (henceforth, 'faint') and 679 galaxies in the  $-22.0 < M_I \leq -21.0$  (henceforth, 'bright'). Further, we investigate morphological dependences of our results by splitting our sample into early and late-type galaxies using a publicly available morphology catalog for GOOD-South<sup>10</sup> (Griffiths et al. 2012, in prep). The sample is dominated by late-type galaxies ( $n_{Sersic} < 1.5$ ) accounting for 1938 objects, 6 times the number of early-type galaxies ( $n_{Sersic} > 2.5$ ). 1915 galaxies in the sample have  $v - i < 1$ . The mean half light radius ( $R_{50}$ ) of the sample is  $0.45''$ . The mean half light diameter is thus 7 times the angular size of the resolution element (PSF FWHM in the  $i$  band is  $\sim 0.11''$ ).

### 3. METHODS

#### 3.1. Measuring the color gradients in galaxies

ACS science images are in counts/sec, while the weight maps are inverse variance maps (i.e.,  $1/\sigma_f^2$ ). Flux calibration of the science and weight postage stamp ACS images of each source is performed using the ACS zeropoints listed<sup>11</sup>. These contain the variance from the sky noise, read-out noise and dark currents.

Further, because the pixels are correlated, the actual noise is higher than the theoretical noise in the weight files (Casertano et al. 2000). We account for this by computing the noise in empty patches (away from the object and whose size is larger than the correlation length scale) in the science image and we calculate the ratio of this measured noise value to the theoretical noise value. The mean ratio is 0.6. The noise in the weight images is then rescaled by this ratio to give a more accurate estimate of the noise in the pixels due the background and instrument. The Poisson uncertainty from pixels in the source itself is then added.

The  $v$  and  $i$  images are PSF-matched using the *ip\_diffim*<sup>12</sup> image mapping software currently in the pipeline of LSST. This is a version of the Higher Order Transform of Psf and Template Subtraction code (*Hotpants*<sup>13</sup>). This code imple-

ments the algorithm of Alard (1999) and Alard & Lupton (1998) for image subtraction by finding the kernel that is needed to map a input image to a template image. The kernel is decomposed into a set of basis functions, usually Gaussians of varying FWHM. The process is thus a linear least-squares problem and can be solved via matrix inversion. This process matches the PSFs of the two input images given an appropriate kernel. Since the PSF varies spatially in all the images, the code models the kernel as a spatially varying function as well. A bounding box is chosen for each galaxy, centred on the central pixel of each galaxy (as found above) in order to avoid masked or bad pixels from affecting the procedure. A similar process is used to PSF-match the variance images.

The color gradient across the galaxy is measured as:

$$\delta(v - i) = (v - i)_{R_{50} \leq r < 2R_{50}} - (v - i)_{r < R_{50}} \quad (1)$$

where  $(v - i)_{r < R_{50}}$  is the  $v - i$  color inside  $R_{50}$  and  $(v - i)_{R_{50} \leq r < 2R_{50}}$  is the  $v - i$  color between  $r \geq R_{50}$  and  $r < 2R_{50}$ . The upper limit of  $2R_{50}$  is validated by determining the radial dependence of the signal-to-noise ratio (SNR) in volume-limited subsamples of galaxies out to  $z \sim 3$ . In galaxies at  $z \sim 2.5$ , the SNR declines significantly beyond  $2.5R_{50}$ . In addition, when these galaxies at  $z \sim 2 - 3$  are stacked, the SNR in the annulus  $1.5R_{50} < r < 2R_{50}$  is 9.0 and falls below 2.0 for  $r > 2.5R_{50}$ . See Section 4.3 for more details.

Photometric errors in each pixel are propagated from the variance images in order to provide an uncertainty on the measurement of the color gradient for each galaxy.

#### 3.2. Effect of galaxy size on the measured color gradient

We perform simulations to determine how the input galaxy size in these objects impact the accuracy with which a color gradient can be recovered for these galaxies. We simulate mock disk galaxies with an exponential profile at a given redshift  $z$  and with a range of values of  $R_{50}$ . Luminosities are assigned to each particle in the disk using SEDs generated from the Bruzual & Charlot 2003 (BC03) stellar population synthesis models. These luminosities are assigned to the stellar particles such that an input color gradient exists in the galaxy between  $r < R_{50}$  and  $R_{50} < r < 2 \times R_{50}$ . Mock images in the ACS  $v$  and  $i$  filters are made by redshifting the SEDs to the redshift of the galaxy and convolving the SEDs with the ACS filters. The images are then pixelated to the ACS pixel scale ( $0.03''$ /pixel in the drizzled images) and smoothed with a Gaussian kernel of FWHM  $3.7 \times 3.7$  pixels in order to simulate the resolution of the actual ACS images (PSF FWHM in  $i$  band  $\sim 0.11''$ ).

The results of this simulation are shown in Figure 3 where we plot the fractional error in the recovered color gradient  $v - i$  as a function of the input  $R_{50}$  of the galaxy for a range of color gradients which are assigned initially to the galaxy. As expected, the fractional error increases as the galaxy size decreases. However, for  $R_{50} < 0.3''$ , the fractional error exceeds 0.2 and increases sharply beyond

<sup>10</sup> [www.ugastro.berkeley.edu/~rgriffit/gems\\_v\\_z\\_public\\_catalog\\_5.0.fits](http://www.ugastro.berkeley.edu/~rgriffit/gems_v_z_public_catalog_5.0.fits)

<sup>11</sup> [http://archive.stsci.edu/pub/hlsp/goods/v2/h\\_goods\\_v2.0\\_rdm.html](http://archive.stsci.edu/pub/hlsp/goods/v2/h_goods_v2.0_rdm.html)

<sup>12</sup> <http://dev.lsstcorp.org/trac/>

<sup>13</sup> <http://www.astro.washington.edu/users/becker/hotpants.html>

this value. We thus use  $R_{50} > 0.3''$  (half light diameter  $\sim 5.5 \times \text{FWHM } PSF_i$ ) as a benchmark to select galaxy sizes in our sample. Note that this size limit is more conservative than the selection of  $d > 1.6 \times \text{FWHM}$  ( $d$  being the typical galaxy size) in the COSMOS survey (Scoville et al. 2007; Koekemoer et al. 2007) for galaxy shape measurements for weak lensing (Leauthaud et al. 2007).

#### 4. RESULTS

##### 4.1. Observed color gradients and their dependence on galaxy properties

Figure 4 illustrates the dependence of the observed color gradient on galaxy properties. We observe the color gradient increasing with both the  $v$  and  $i$  band apparent magnitudes out to  $\sim 25.5$  magnitudes. This implies that fainter galaxies are progressively redder in their outskirts than in their centres, while brighter galaxies have a negative color gradient, implying that their outskirts are bluer than their centres. The color gradient also increases rapidly for galaxies fainter than  $i = 22.5$  magnitudes. A similarly large, though less steep rise in the color gradient is observed in the  $v$  band magnitude. We observe a decreasing color gradient with increasing  $R_{50}$  i.e. small galaxies have bluer cores compared to their outskirts, but as the galaxy size increases, the core becomes progressively redder compared to the outskirts, resembling local early-type galaxies more closely.

The trend with redshift is also very remarkable. There is little evolution in the color gradient or in its scatter out to  $z \sim 1$ . However, beyond  $z \sim 1$ , there is a sharp increase in the color gradient out to  $z \sim 3$ , implying that galaxies become bluer in their core relative to their outskirts. This can be interpreted as follows. For  $z < 1$ , we are measuring rest-frame optical colors which probe older stellar populations. For  $z > 1$ , we are measuring rest-frame UV colors which are more sensitive to the bluer and younger stellar populations. In particular, we observe bluer colors in the centres of galaxies relative to the outskirts above  $z \sim 1$ . There is an indication also that the increasing trend flattens out from  $z \sim 2$  to  $z \sim 3$ . The redshift evolution of the median color gradient for  $0.5 < z \leq 3.0$  can be described by the parametric function  $\delta_{(v-i)}(z) = -0.033z^3 + 0.119z^2 + 0.045z - 0.093$  (a bin size of  $\Delta z = 0.5$  is used, with the data points in Figure 4 corresponding to the centres of the bins). There is also a strong dependence of the gradient on  $(v-i)$  color. The bluest galaxies have a positive color gradient  $\sim 0.25$  magnitudes i.e. their cores are bluer relative to their outskirts, while redder galaxies have redder cores relative to their outskirts, consistent with local S0/Sa galaxies. The trend with absolute magnitude is weak although there is an indication that the color gradient increases and its scatter decreases slightly towards the lowest luminosities. Finally, we examine the trend of the gradient with morphological type. There is not a strong dependence but a suggestion of a slight decrease in the color gradient with increasing Sersic index. For  $n < 1.5$  (late-type galaxies), there is an indication that these galaxies have bluer centres compared to early-type galaxies ( $n > 2.5$ ), but the trend is quite weak for the whole sample. We examine the dependence of the color gradient on galaxy morphology in more detail below.

##### 4.2. Dependence on morphological type

In order to investigate any dependence of galaxy morphology on the results, we perform a similar analysis on late-type galaxies ( $n_{\text{Sersic}} < 1.5$ ) and early-type ( $n_{\text{Sersic}} > 2.5$ ) in the sample. The results are shown in Figure 5. The trends of  $\delta_{(v-i)}$  with galaxy properties for late-type galaxies are very similar to the trends in the full galaxy sample since the latter is dominated by late-type galaxies. The trends are also qualitatively similar between early and late-type objects but there are some notable differences. The color gradient for late-type galaxies increases monotonically from the brightest to the faintest magnitudes ( $i_{AB} \sim 25.5$ ). The trend with  $i_{AB}$  apparent magnitude for early-type galaxies shows some differences compared to late-type galaxies. The median color gradient for early-type galaxies shows very little variation with magnitude up to  $i_{AB} = 22.5$  but the relation also has a larger scatter than for late-types. Beyond  $i_{AB} = 22.5$ , the median  $\delta_{(v-i)}$  increases sharply up to 0.15 magnitudes at  $i_{AB} = 23.5$ , indicating that the cores of early-type galaxies become bluer compared to their outskirts. Beyond  $i_{AB} = 23.5$ , the median  $\delta_{(v-i)}$  shows little variation with  $i_{AB}$  magnitude. The variation of the color gradient in early-type galaxies with the  $v_{AB}$  magnitude is similar to that in late-types, with both galaxy types showing little variation of  $\delta_{(v-i)}$  with  $v_{AB}$  up to  $v_{AB} = 23.5$ . However, the scatter in the relation at the faintest magnitudes ( $i_{AB} > 23.5$ ) is much larger for early-type galaxies.

There is some difference in the evolution of the color gradient with color. Bluer early-type galaxies ( $v-i < 1.0$ ) have a color gradient which shows little variation with color but for  $v-i > 1.0$ ,  $\delta_{(v-i)}$  decreases towards redder early-type objects. The bluest early-type galaxies have a median  $\delta_{(v-i)}$  that is closer to zero indicating that the bulge and disk components are not as well separated as for late types. By comparison, the bluest late-type objects have cores which are bluer by as much as 0.25 magnitudes compared to their outskirts, and  $\delta_{(v-i)}$  then decreases monotonically with  $v-i$  color. Both the reddest early-type and late-type galaxies have cores which are redder by as much as 0.15 magnitudes compared to their outskirts.

The color gradient relation with  $R_{50}$  has a larger scatter for early-type galaxies than for late-types. There is an indication of a reduced color gradient for larger early-type galaxies and this trend is also observed for late type galaxies although the scatter in the relation is larger for early-type objects. These objects with large  $R_{50}$  are probably similar to local early-type galaxies that have red cores. Late-type galaxies also show little or no evolution in the color gradient with luminosity (as in the case of the full sample) but early-type galaxies do show an indication that the gradient increases, from the intrinsically brightest objects at  $M_I = -23.0$  which show bluer outskirts, to the lowest luminosities where galaxies have slightly redder outskirts compared to their centres.

The trends with redshift are broadly similar for early and late-type galaxies, although the scatter in the trend for the early-type galaxies is larger. Early-type objects show little or no evolution in their color gradient below  $z \sim 1$ , consistent with the results of Ferreras et al. (2005). However, for  $z > 1$ , their color gradient becomes increasingly

positive before flattening off around  $z \sim 1.5$ . This implies that early-type galaxies become bluer in their centres at high redshifts, in marked contrast to their local counterparts. Finally, in the redshift interval  $z = 2.5 - 3.0$ ,  $\delta_{(v-i)}$  is  $+0.17$  for early-type galaxies and  $+0.24$  for late-type galaxies. This indicates that at high redshifts, the cores of late-type objects not only become progressively bluer relative to their outskirts but that the difference between the color of the outskirts and the color of the core becomes stronger in late-type galaxies than it does for early-type galaxies.

#### 4.3. *The stacked radial color variation in galaxies*

We investigate further the observed evolution of the color gradient with redshift by measuring the radial variation of color in two luminosity ranges  $-21.0 < M_I \leq -20.0$  and  $-22.0 < M_I \leq -21.0$ . We measure the  $v - i$  color in successive radial annuli for each galaxy in each absolute magnitude interval. We select galaxies in the range  $0.30 < R_{50} < 0.40$  in order to verify the measurement accuracy, since these galaxies will be representative of objects at the highest redshifts. Galaxies in each of these absolute magnitude intervals have the radius of their annuli scaled by  $R_{50}$  before the galaxies are stacked. We have performed tests to ensure that our outermost annuli are not biased by the color of the background. For  $z \sim 2.0 - 3.0$ , the SNR for the stacked galaxies in the outermost annulus ( $r = 1.5 - 2R_{50}$ ) is 9.0, and is always above 2.0 for any radius below  $2R_{50}$ . Beyond  $2R_{50}$ , the SNR decreases sharply below 2.0.

The results are shown in Figure 6. In both luminosity intervals, we observe the color gradient becoming progressively more positive for  $z > 1$  i.e., showing increasingly bluer cores relative to the outskirts. At  $z = 0.5 - 1.0$ , the cores of galaxies ( $r < 0.5R_{50}$ ) are slightly redder on average compared to their outskirts by 0.05-0.1 magnitudes in both luminosity intervals. However, at  $z = 2.5 - 3.0$  and  $-21.0 < M_I \leq -20.0$ , the core is bluer by 0.6 magnitudes (at a  $16\sigma$  significance level) compared to the outskirts ( $r = 1.5 - 2R_{50}$ ). In the intrinsically brighter galaxies ( $-22.0 < M_I \leq -21.0$ ) in the same redshift interval, the core is bluer by 0.42 magnitudes compared to the outskirts. We remark that the radial trends are qualitatively similar in both luminosity intervals although the exact magnitude of the color difference between the core and the outskirts can vary.

Another very important point to emphasise is that for both luminosity ranges, the color in the outskirts of the galaxy changes much less than the internal color. The color at  $r \sim 1.5 - 2.0R_{50}$  changes by approximately 0.2 magnitudes between  $z \sim 0$  and  $z \sim 3.0$ , for galaxies in  $-22.0 < M_I \leq -21.0$  (and 0.05 magnitudes in  $-21.0 < M_I \leq -20.0$ ). In comparison, in the interior ( $r < 0.5R_{50}$ ), the color changes by as much as 0.77 magnitudes (0.57 magnitudes at  $-21.0 < M_I \leq -20.0$ ). This indicates that as the star formation rate in galaxies increases towards  $z \sim 3$  (galaxies becoming bluer), it is the central regions of galaxies where this increase is most marked, possibly due to increased gas densities in the central regions.

#### 4.4. *Biases in the color gradient arising from spectroscopic redshifts*

In Figure 7, we investigate any bias in the evolution of the color gradient when using spectroscopic redshifts as opposed to photometric ones. The trend of the color gradient with the spectroscopic redshift is similar to the trend with the photometric redshift. However, we find that, up to  $z \sim 1$ , the median color gradient for the spectroscopic sample is lower by 0.04 magnitudes compared to the photometric sample and it is lower by 0.07 magnitudes at  $z \sim 2$ . This can be explained by the different color distributions of the two samples, with the spectroscopic sample (which is color-selected) being redder by 0.2 magnitudes than the photometric one at  $z \sim 1$ . This bias is also consistent with the strong color dependence we found for the color gradient (Figure 4), with redder galaxies having a less positive color gradient.

## 5. DISCUSSION

### 5.1. *Interpretation in terms of galaxy evolution*

The observed evolution with redshift is consistent with the picture of galaxies being increasingly star-forming at higher redshifts. Importantly, our results suggest that the star formation becomes increasingly dominant in the cores of galaxies relative to their outskirts, at higher redshifts. This is consistent with the star formation being concentrated in the nuclei of galaxies, possibly driven by higher gas densities in the centre. There are several studies that support the picture of very high star formation rates in  $z \sim 1 - 3$  galaxies being driven by high gas densities and self-regulated star formation i.e., the star formation determines the average thermal and turbulent pressure in the inter-stellar medium (ISM), which in turn affects the star formation rate. Lehnert et al. (2009) have proposed that the large  $H\alpha$  line widths observed in  $z \sim 1 - 3$  intensely star-forming galaxies are driven by self-regulated star formation through the mechanical energy liberated by massive stars. They also found that the intensity of the star formation in these distant galaxies is as high as that observed in local starbursts (e.g., M82), but the star formation occurs on a much larger physical scale, and it is maintained by large gas fractions and high mass-surface densities. These  $H\alpha$  line widths do not appear to be driven by either cosmological accretion (Le Tiran et al. 2011a) or gravitational instabilities.

Further, Le Tiran et al. (2011b) also stacked rest-frame optical emission lines such as  $[\text{SiII}]\lambda\lambda 6716, 6731$  and  $[\text{OI}]\lambda 6300$ , of about 50 color-preselected galaxies at  $z = 1.2 - 2.6$  which also had high  $H\alpha$  surface brightnesses, in order to investigate how gas properties scale with the star formation intensity. They found that their high redshift sample showed trends similar to those observed in local galaxies where gas pressures scale with the star-formation intensity. In particular, they found higher gas densities (and hence pressures) in intensely star-forming regions compared to fainter diffuse gas, with values comparable to starburst regions and the diffuse ISM in nearby galaxies. In their stacked sample, they found that in addition to single narrow components of  $H\alpha$  and  $[\text{NII}]\lambda\lambda 6548, 6583$ , broad lines in  $H\alpha$  and  $[\text{NII}]$  were also observed. These broad lines are only significantly detected in the stacks with the highest star-formation intensities. This broad emission supports the hypothesis that outflows, rather than active galactic nuclei, are closely linked to the high

star-forming intensities.

Thus, if very high gas densities are indeed present in the centres of  $z > 1.5$  galaxies, this would support the hypothesis of very strong star formation which is driven by feedback and self-regulation and is concentrated in the centres of galaxies as opposed to their outskirts. That would be consistent with the color gradients we observe at these high redshifts.

### 5.2. Implications for shear measurements

The observed trends in the color gradient discussed above are important in the context of weak lensing galaxy shape measurements. Indeed, the faint distant galaxies targeted by weak lensing surveys are convolved by the instrumental PSF which is a function of wavelength (generally being broader at longer wavelengths). Hence, galaxies of a given intrinsic shape (and color) but with different color gradients will have different observed shapes. Uncovering the original galaxy shape thus requires, in principle, a knowledge of the PSF variation with wavelength (as studied by Cypriano et al. 2010) and also of the galaxy's intrinsic color gradient.

In the case of ground-based observations such as those conducted with CFHT/Megacam, the new wide-field imager VST/OmegaCam, and the upcoming DES and HSC projects, the limited spatial resolution may not allow an identification of the color gradients of galaxies. However, the PSF of ground-based observations is well characterized in different bands, and an accurate measurement of inte-

grated galaxy colors can be made. The variation of the color gradient with galaxy color and redshift that we have identified in this paper, should allow us to build a model for correcting the PSF smearing by including the galaxy color and photometric redshift in the shape measurement scheme.

In the case of space-based observations, color gradients can be easily measured when multi-band information is available, as demonstrated here, so modelling the correction of the PSF smearing should not be a difficult problem for resolved multi-band observations. These observations can be used to quantify the size of the bias as a function of galaxy properties, which in turn can be used to correct the bias. In a forthcoming paper, we will investigate these different issues for both the ground and space-based observations. We will propose a model that could potentially correct the shape measurement bias, taking into account the variation of the color gradient with galaxy properties as presented in this work.

### 6. ACKNOWLEDGEMENTS

NW thanks L. Tasca for provided the cutout images for this analysis, O. Ilbert for useful discussions and A. Becker and R. Owen for help and advice on using code from the LSST Trac. We thank Y. Mellier and H. Hoekstra for their helpful suggestions. NW acknowledges support from the Centre National d'Études Spatiales (CNES) and the Centre National de la Recherche Scientifique (CNRS). JPK acknowledges support from CNRS and CNES.

### REFERENCES

- Abazajian, K. N. et al., 2009, *ApJS*, 182, 543  
 Alard C., & Lupton R.H., 1998, *ApJ*, 503, 325  
 Alard C., 1999, *astro-ph/990311*  
 Bakos J., Trujillo I. & Pohlen M., 2008, *ApJ*, 683, L103  
 Balestra I. et al., 2010, *A&A*, 512, 12  
 Bertin E. & Arnouts S., 1996, *A&AS*, 117, 393  
 Bruzual G. & Charlot, S., 2003, *MNRAS*, 344, 1000  
 Cardamone C.N. et al., 2010, *ApJS*, 189, 270  
 Casertano S. et al., 2000, *AJ*, 120, 2747  
 Cypriano, E. S. et al., 2010, *MNRAS*, 405, 494  
 den Brok M. et al., 2011, *MNRAS*, 414, 3052  
 Ferreras I. et al., 2005, *ApJ*, 635, 243  
 Giavalisco M. et al., 2004, *ApJ*, 600, 103  
 Gonzalez-Perez V., Castander F.J. & Kauffmann G., 2011, *MNRAS*, 411, 1151  
 Green J. et al., *Wide-Field InfraRed Survey Telescope (WFIRST) Interim Report*, 2011, arxiv: 1108.1374  
 Griffiths R. et al., 2012, in preparation  
 Groth E. J., Kristian J. A., Lynds R., O'Neil E. J. Jr., Balsano R., & Rhodes J., 1994, *BAAS*, 185, 53.09  
 HSC Collaboration, *Hyper Suprime-Cam Design Review*, 2009.  
 Koekemoer A. M., 2007, *ApJS*, 172, 196  
 Laureijs R. et al., 2011, *Euclid Definition Study Report*, arXiv:1110.3193  
 Leauthaud A. et al., 2007, *ApJS*, 172, 219  
 Lee J. H., Lee M. G., Park C., Choi Y.-Y., 2008, *MNRAS*, 389, 1791  
 Lehnert M.D. et al., 2009, *ApJ*, 699, 1660  
 Le Tiran L. et al., 2011a, *A&A*, 530, 6  
 Le Tiran L. et al., 2011b, *A&A*, 534, 4  
 LSST Science Collaborations, 2009, *LSST Science Book, Version 2.0*, arXiv:0912.0201  
 Park C. et al., 2007, *ApJ*, 658, 898  
 Popesso P. et al., 2009, *A&A*, 494, 443  
 Rhodes J., Refregier A., & Groth E. J., 2000, *ApJ*, 536, 79  
 Scoville, N. Z. et al., 2007, *ApJS*, 172, 1  
 Simard L., Willmer C. N. A., Vogt N. P., Sarajedini V. L., Phillips A. C., Weiner B. J., Koo D. C., Im M., Illingworth G. D., Faber S. M., 2002, *ApJS*, 142, 1  
 SNAP Collaboration, *Supernova / Acceleration Probe: A Satellite Experiment to Study the Nature of Dark Energy*, 2004, arxiv:astro-ph/0405232  
 Suh H. et al., 2010, *ApJS*, 187, 374  
 Tortora C. et al., 2010, *MNRAS*, 407, 144  
 Tortora C. et al., 2011, *MNRAS*, 418, 1557  
 Voigt L.M. et al., 2011, arXiv:1105.5595  
 Welikala N. et al., 2008, *ApJ*, 677, 970  
 Welikala N. et al., 2009, *ApJ*, 701, 994  
 Wester W. et al., 2005, *ASPC*, 339, 152

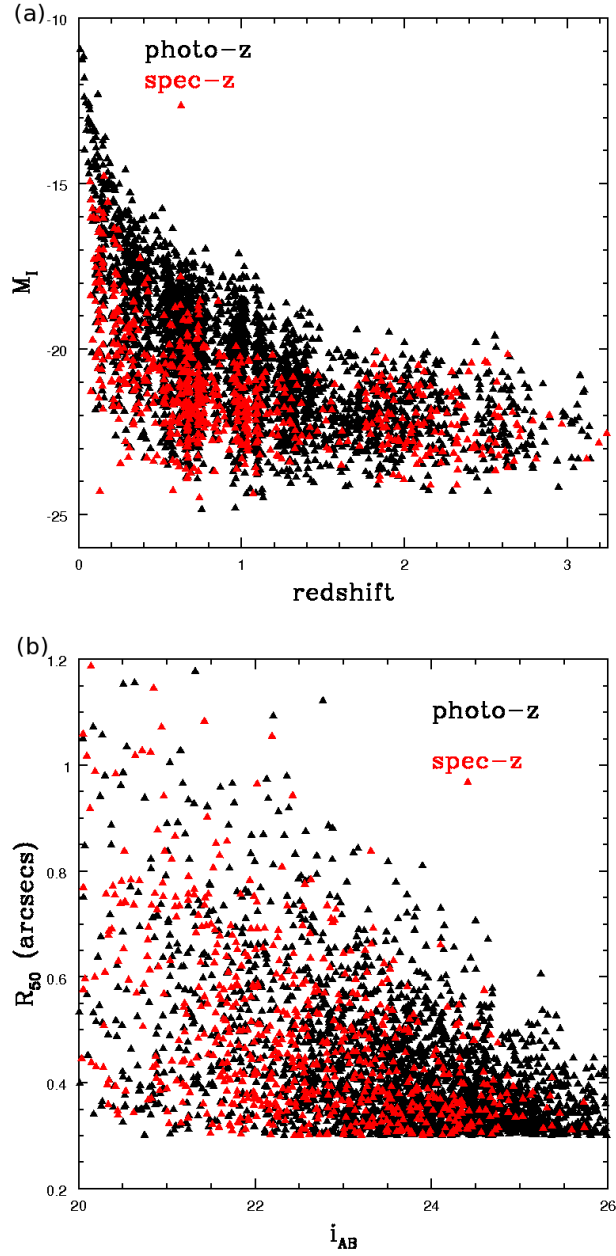


FIG. 1.— Selection of the photometric (in black) and spectroscopic samples (red) in GOODS-South that were used in this study. (a)  $M_I$  as a function of redshift and (b)  $R_{50}$  versus magnitude.

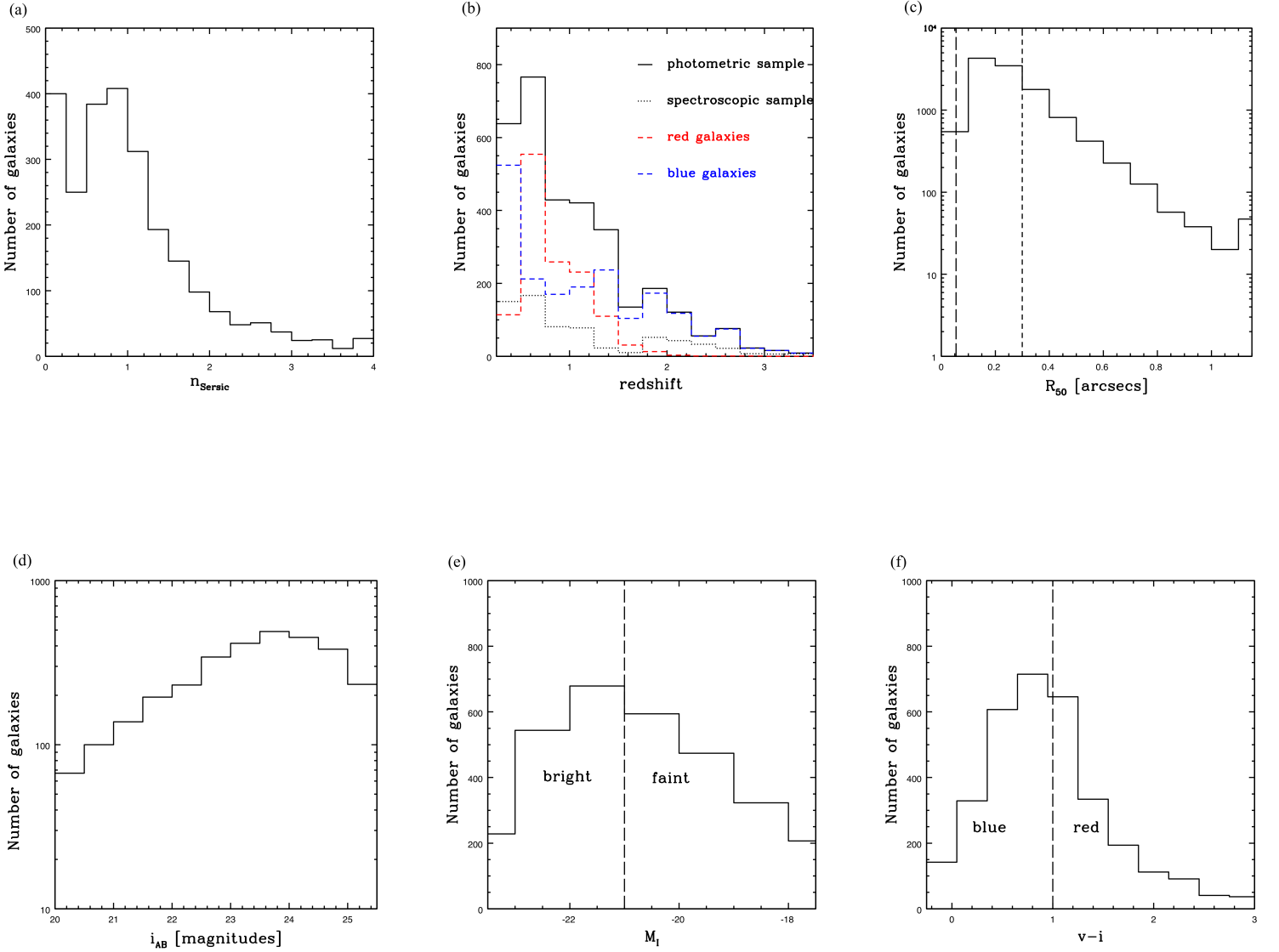


FIG. 2.— The distribution of the photometric properties of the galaxy sample in this study. The panels show (a) the distribution of the Sersic index  $n_{Sersic}$  (b) the redshift distribution, showing the contribution of the photometric sample (solid black line), the spectroscopic sample (dotted black line), the red galaxies in the photometric sample (with  $v - i \geq 1.0$ , red dashed line) and the blue galaxies ( $v - i < 1.0$ , blue dashed line) (c) the distribution of the half light radius  $R_{50}$  (d) the  $i_{AB}$  magnitude distribution (e) the  $I$  band absolute magnitude distribution (f) the distribution of  $v - i$  color.

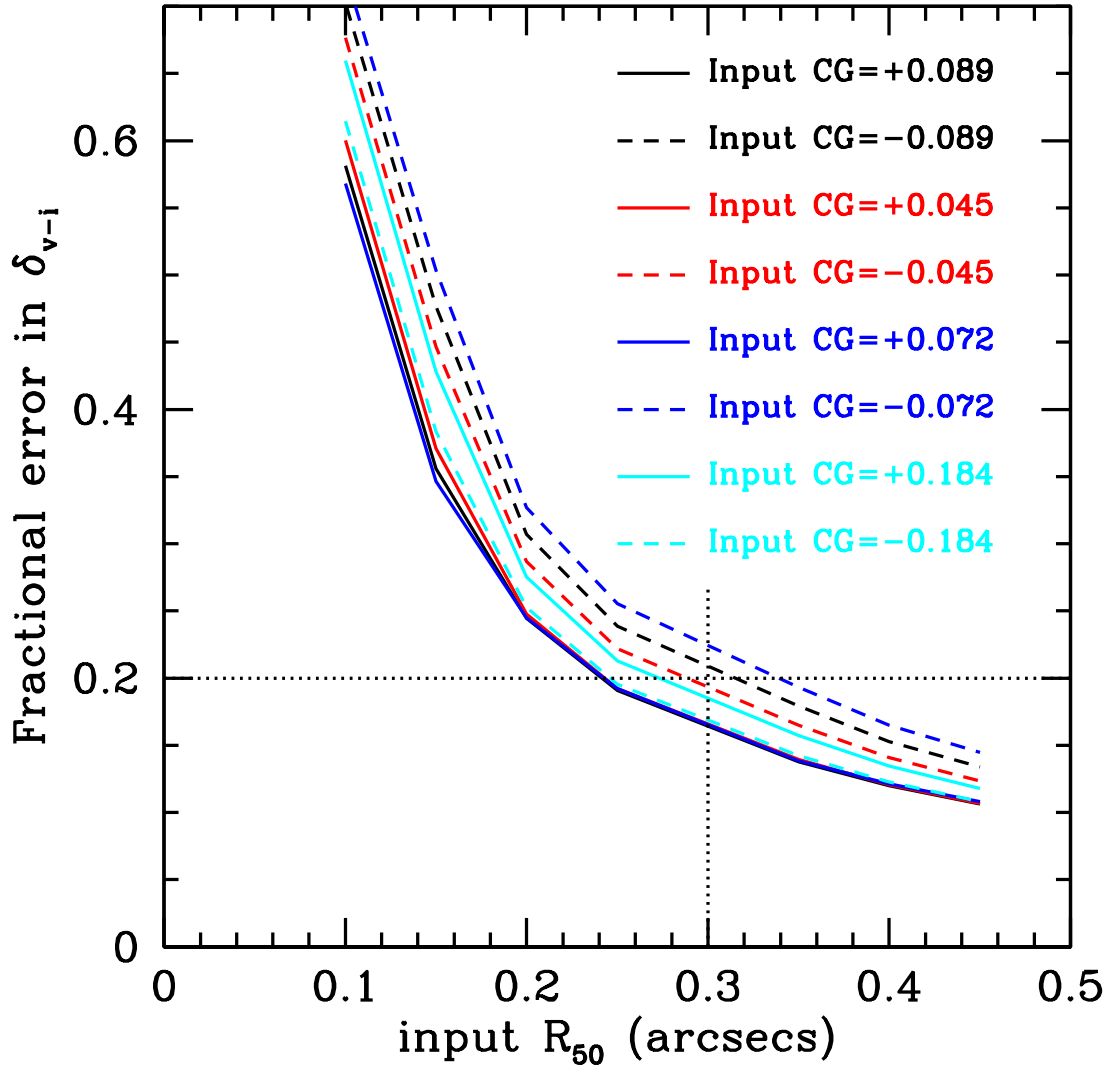


FIG. 3.— Fractional error in the recovered  $v - i$  color gradient as a function of the half light radius  $R_{50}$  for simulated disk galaxies with an exponential radial surface brightness distribution. Marked is our selection in  $R_{50}$  corresponding to a fractional error of 0.2 in recovering the input gradient (dotted line).  $v$  and  $i$  band images of disk galaxies at  $z = 0.5$  have been simulated with various color gradients assigned between  $r < R_{50}$  and  $R_{50} \leq r < 2R_{50}$ . The images have the same pixel scale as the drizzled ACS  $i775$  band images ( $0.03''/\text{pixel}$ ). After assigning the input color gradient, the image of the galaxy is smoothed by a Gaussian kernel of  $3.7 \times 3.7$  pixels in order to match the PSF FWHM in the  $i775$  band ( $\sim 0.11''$ ). The luminosities in each pixel are derived from the Bruzual & Charlot (BC03) stellar population synthesis models.

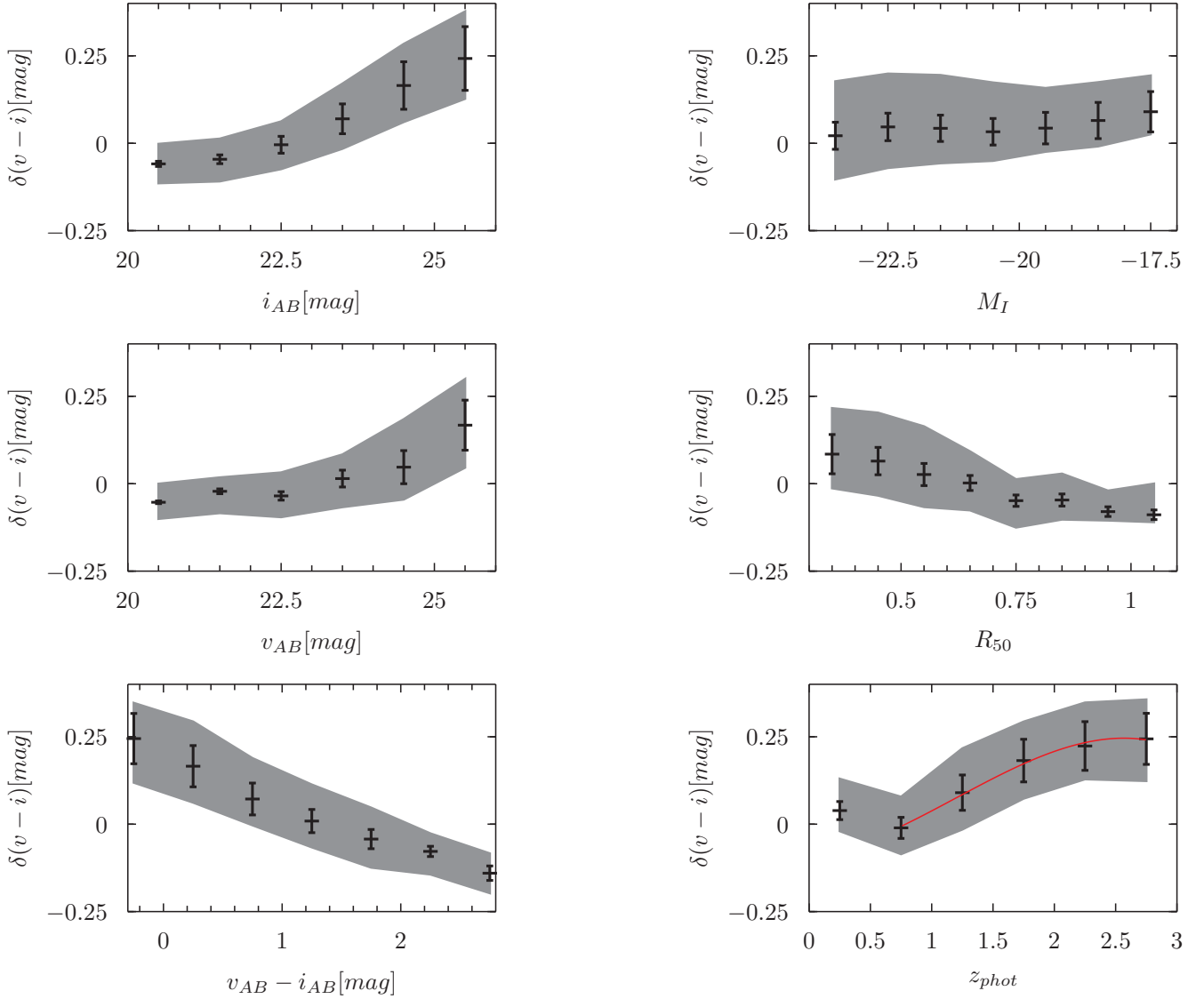


FIG. 4.— Dependence of the color gradient  $\delta(v-i)$  on galaxy properties in the GOODS-South photometric sample. The shaded region in each panel is bounded by the 25th and 75th percentile of the measured color gradient. The panels show the dependence of the gradient on (a) the  $i_{AB}$  apparent magnitude (b) the  $I$  band absolute magnitude (c) the  $v_{AB}$  apparent magnitude (d) the galaxy half light radius  $R_{50}$  (e)  $v-i$  color (f) the photometric redshift  $z_{phot}$ . The redshift evolution of the median color gradient for  $0.5 < z \leq 3.0$  is described by the polynomial function  $\delta_{(v-i)}(z) = -0.033z^3 + 0.119z^2 + 0.045z - 0.093$  (red line). A bin size of  $\Delta z = 0.5$  is used and the data points correspond to the centres of the bins.

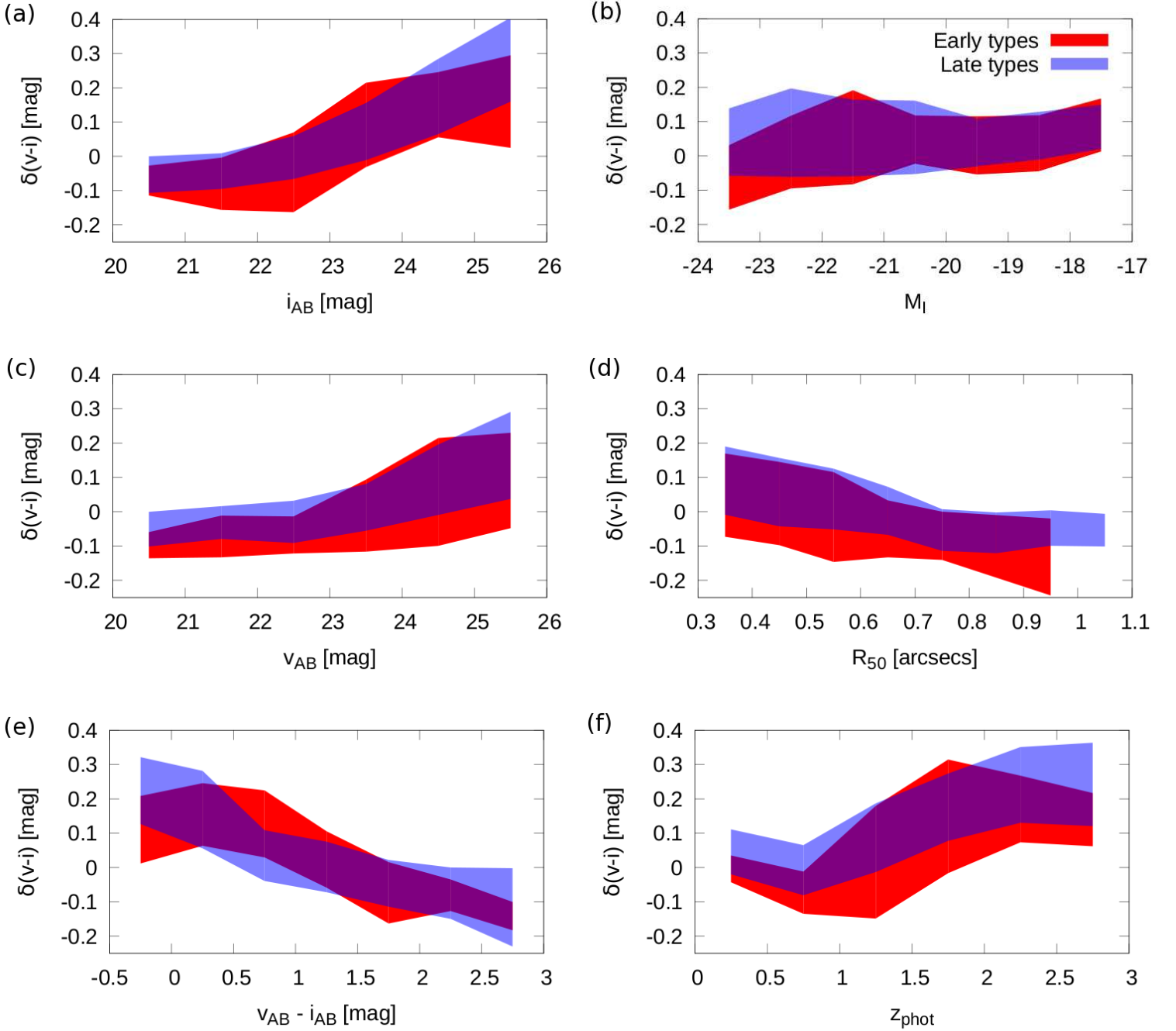


FIG. 5.— Morphological type dependence of the trends in the color gradient. The panels show the dependence of the gradient on (a) the  $i_{AB}$  apparent magnitude (b) the  $I$  band absolute magnitude (c) the  $v_{AB}$  apparent magnitude (d) the galaxy half light radius  $R_{50}$  (e)  $v - i$  color (f) the photometric redshift  $z_{phot}$ . The red shaded region corresponds to early-type galaxies in the sample and the blue shaded region corresponds to late-type galaxies. The shaded region in each panel is bounded by the 25th and 75th percentile of the color gradient in the sample being studied.

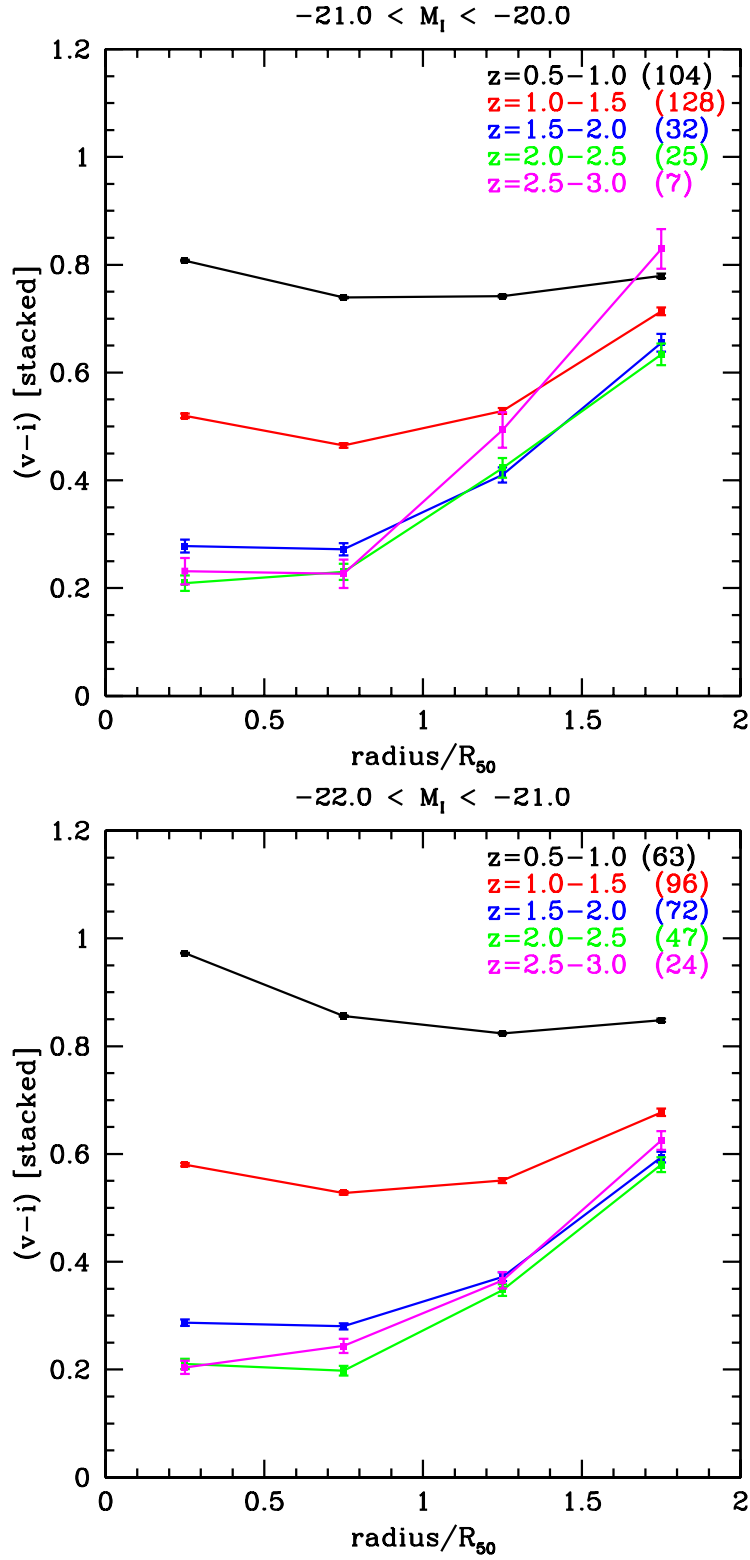


FIG. 6.— Evolution of the radial variation of  $v - i$  color in stacked galaxies with redshift for two different luminosity intervals. Galaxies are selected to have  $R_{50} = 0.30 - 0.40$  and to be in two intervals of absolute magnitude  $-21.0 < M_I \leq -20.0$  (faint bin, top panel) and  $-22.0 < M_I \leq -21.0$  (bright bin, bottom panel). Galaxies in each of these absolute magnitude intervals have the radius of their annuli scaled by their  $R_{50}$ , before the galaxies are stacked. The number of galaxies in each redshift bin is labelled in parentheses. At  $z \sim 2.0 - 3.0$ , the SNR for the stacked galaxies in their outermost annuli ( $r = 1.5 - 2R_{50}$ ) is 9.0, and is above 2.0 for all radii up to  $r = 2R_{50}$ .

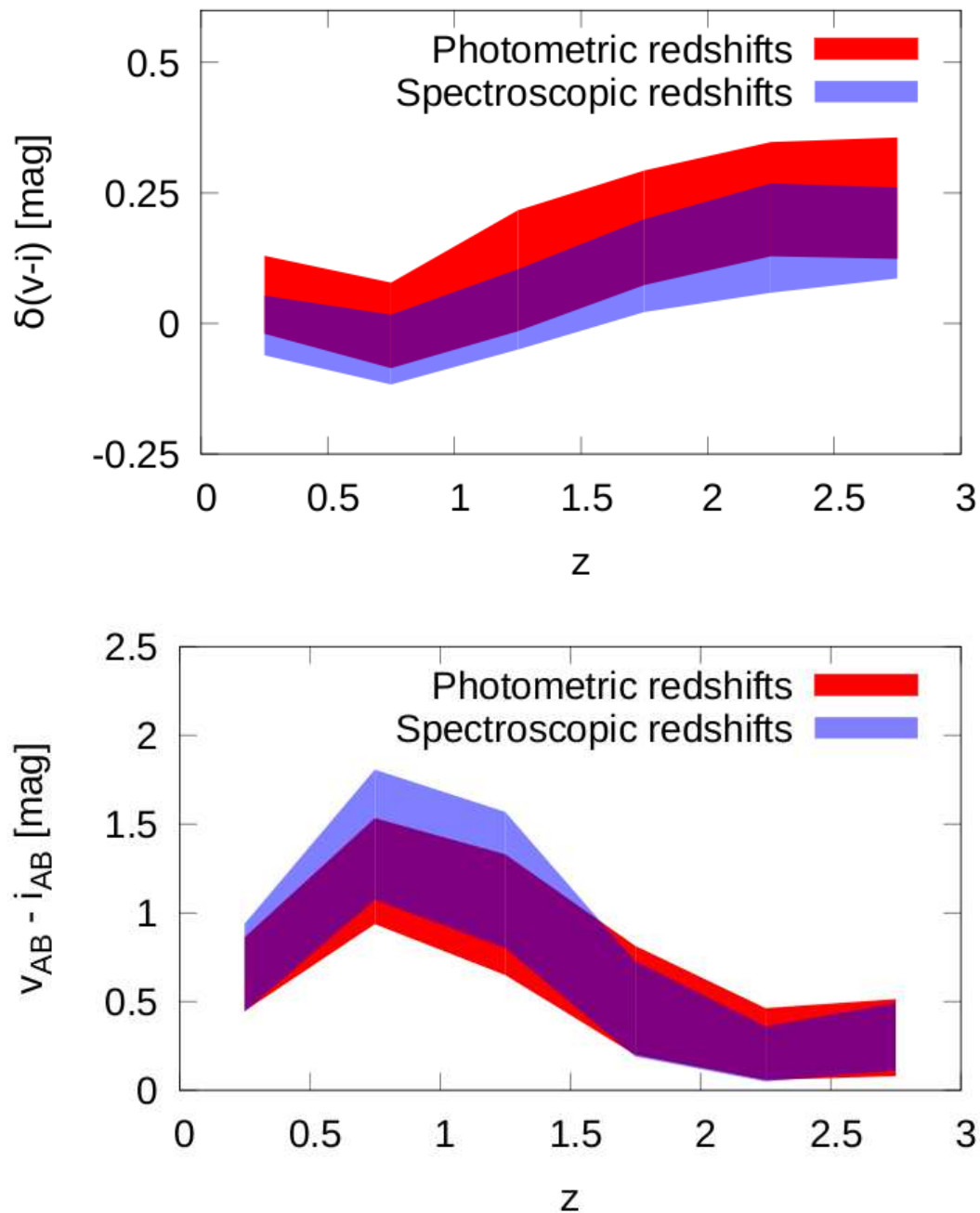


FIG. 7.— Top panel: the color gradient  $\delta(v - i)$  as a function of redshift when (a) photometric redshifts are used (red shaded region) and (b) only spectroscopic redshifts are used (blue shaded region). The spectroscopic redshifts have been derived from the GOODS-VIMOS spectroscopic campaign (Balestra et al. 2009). The bottom panel shows the color distribution  $v - i$  of the sample as a function of the photometric redshift (red shaded region) and the spectroscopic redshift (blue shaded region).